Chinese Journal of Catalysis 46 (2023) 11–27

available at www.sciencedirect.com

ScienceDirect

journal homepage: www.sciencedirect.com/journal/chinese-journal-of-catalysis

Article

Hydrogen transfer reaction contributes to the dynamic evolution of zeolite-catalyzed methanol and dimethyl ether conversions: Insight into formaldehyde

Shanfan Lin [a,c], Yuchun Zhi [a], Wenna Zhang [a], Xiaoshuai Yuan [d], Chengwei Zhang [a,c], Mao Ye [a], Shutao Xu [a], Yingxu Wei [a,*], Zhongmin Liu [a,b,c,*]

[a] *National Engineering Research Center of Lower-Carbon Catalysis Technology, Dalian National Laboratory for Clean Energy, iChEM (Collaborative Innovation Center of Chemistry for Energy Materials), Dalian Institute of Chemical Physics, Chinese Academy of Sciences, Dalian 116023, Liaoning, China*

[b] *State Key Laboratory of Catalysis, Dalian Institute of Chemical Physics, Chinese Academy of Sciences, Dalian 116023, Liaoning, China*

[c] *University of Chinese Academy of Sciences, Beijing 100049, China*

[d] *Research Center for Energy Strategy, Dalian Institute of Chemical Physics, Chinese Academy of Sciences, Dalian 116023, Liaoning, China*

ARTICLE INFO

Article history:
Received 29 September 2022
Accepted 10 November 2022
Available online 5 March 2023

Keywords:
Methanol-to-Olefins
Dimethyl ether
Hydrogen transfer
Formaldehyde
Deactivation

ABSTRACT

Formaldehyde (HCHO), generating from hydrogen transfer (HT) of reactant, is significant for autocatalysis initiation and deactivation in methanol-to-olefins (MTO), but hitherto, its evolution throughout the reaction has not been thoroughly revealed. Herein, by the established colorimetric analysis method, HCHO in the MTO and dimethyl ether (DME)-to-olefins (DTO) reactions over SAPO-34 was *in situ* quantitatively monitored, where HCHO was detected in slight and conspicuous amounts at initial and deactivation stages with semi-conversion, also when co-fed with water or high-pressure H_2. We reveal the weak HT ability of DME relative to methanol, which enables prominent olefins-based cycle and suppresses reactant-induced HT and deactivation in DTO (which is critical for MTO). A complete dynamic reaction network is disclosed, constituting two simultaneous and interplaying pathways: the main reactions for olefin generation as the open-line and HT reactions as the hidden-line. Especially, co-feeding high-pressure H_2 with DME capacitating a long-term and highly efficient operation of DTO by modulating the dynamic reaction network to a more moderate autocatalysis evolution, has great potential in industry application.

1. Introduction

Methanol-to-olefins (MTO) process, the most successful nonpetroleum industrialized route to obtained olefins from any gasifiable carbon-based feedstock (such as coal, natural gas, biomass, carbon dioxide and waste), has been central to research in both academia and industry [1–3]. MTO reaction is a dynamic autocatalytic process with olefin, methylcyclopentenyl (MCP) and aromatic species working as (auto)catalyst: they not only independently guide their respective catalytic cycles but also operate in concert to build a hypercyclic reaction network, efficiently driving methanol conversion [4]. Hydrogen transfer (HT) is the major route for the formation of these autocatalyst (MCP and aromatic) and alkanes byproduct. But its contribu-

* Corresponding author. E-mail: liuzm@dicp.ac.cn (Z. Liu), weiyx@dicp.ac.cn (Y. Wei).

This work was supported by the National Natural Science Foundation of China (21991092, 21991090, 22072148, 21703239, 22002157), the Innovation Research Foundation of Dalian Institute of Chemical Physics (DICP I202121), the National Natural Science Foundation of Liaoning Province (2022-MS-029), the Key Research Program of Frontier Sciences, Chinese Academy of Sciences (QYZDY-SSW-SC024).
https://doi.org/10.1016/S1872-2067(22)64194-9

tion to the dynamic reaction network of MTO has not been well understood, which is critical for the delicate control of the reaction process.

Two HT routes were identified in MTO: one is olefin-induced HT (OIHT) pathway (Scheme 1, R6), which is widely accepted as the mostly happened HT route [5–7]; the other proposed by Lercher *et al*. [5,7–9] is methanol-induced HT pathway (MIHT) with formaldehyde (HCHO) as a key intermediate. Under typical MTO conditions, HCHO can be generated from HT reactions of methanol (Scheme 1, R2–4) [5,10–14], and/or thermal or reactor-wall catalyzed decomposition of methanol (Scheme 1, R1) [15]. Notably, whether dimethyl ether (DME), another C1 reactant as the dehydration product of methanol, can generate HCHO via decomposition or analogous HT reactions (Scheme 1, R7–R11) [14,16,17]) is controversial [17–20]. Previous works revealed the role of HCHO in MTO mainly including two aspects: engaging in the formation of initial C–C bond [8,14,15,21–25] and accelerating catalyst deactivation [5,8,18–20,26,27]. For this reason, scavenging HCHO is considered to make an important contribution to prolonging the catalyst lifetime of MTO in the strategies proposed by Bhan *et al*. [26,28–31]. However, despite these proposals, HCHO has not been directly observed and quantified in these works. The lack of direct quantification of HCHO conceals its production and fate from the initiation to decay of MTO autocatalysis under real rection conditions.

Due to the high reactivity, low concentration, and low sensitivity to flame ionization detector of chromatography [32], HCHO is difficult to be quantitatively detected by conventional methods like other hydrocarbons. For this reason, many works only qualitatively evidence the existence of HCHO in MTO, especially at the initial reaction stage, by MS [8,12,13,25,33,34], GC-MS [16,24,35], GC [16,24,35] and IR [5,15]. Recently, Lercher's group [8,17] adopted an absorption method to quantify HCHO in MTO under short contact time with low conversion conditions. Pan *et al*. [36] employed synchrotron radiation

Yingxu Wei received her PhD in Dalian Institute of Chemical Physics (DICP), Chinese Academy of Sciences (CAS) in 2001. During her service at the Applied Catalysis Laboratory of DICP since graduation, she conducted the postdoctoral study at University of Namur (Belgium) from 2003 to 2004. She has been the group leader of Catalysis and New Catalytic Reactions in National Engineering Laboratory of Methanol to Olefins since 2009 and was promoted to professor in 2011. Over the years, Prof. Wei has undertaken a number of key academic research projects commissioned by NSFC, CAS, MOST, PetroChina and other organizations. She has been involved in the researches on heterogeneous catalysis, methanol to olefins, catalysts and processes of hydrocarbon conversion, and catalytic conversion of methanol and methane derivatives. Over 110 academic papers authored by Prof. Wei have been published in scientific journals home and abroad and more than 60 patents have been applied and granted. She gained the national special support plan for high level talents. She is on the editorial board of the Chinese Journal of Catalysis and works as the editor of Microporous and Mesoporous Materials.

Prof. Zhongmin Liu is the Director of Dalian Institute of Chemical Physics (DICP) and Qingdao Institute of Bioenergy and Bioprocess Technology, Chinese Academy of Sciences (CAS); Director of National Engineering Laboratory for Methanol to Olefins and National Energy Low-carbon Catalysis and Engineering R&D Center.

Prof. Liu has long been working with the catalysis research, process development, and technology transfer in energy conversion and utilization, and made significant achievements. In 2006, as a leading scientist, Professor Liu, together with partners and his colleagues, finished the first industrial demonstration test of methanol to olefin process, named as DMTO. Based on DMTO technology the world's first commercial unit of MTO process was constructed and started to operate by Shenhua group in 2010, which was an important progress for coal to chemicals, and provides a new chance for the substitution of oil by coal. So far, DMTO technology has been licensed to 31 units with a total olefins production capacity of 20.25 Mt/a. And 16 commercial DMTO units have been put into stream with olefins production capacity of 9.30 Mt/a. This breakthrough leads coal to olefins to a new industrial sector in China, greatly changes Chinese light olefins supply, and impacts the light olefins market worldwide. Professor Liu also developed coal-based ethanol production technology, via carbonylation of dimethylether and further hydrogenation, and finished its commercialization by construction of a world's first plant (100KTA) in 2017, which demonstrates a new way for the clean utilization of coal. Up to now, eight DMTE units have been licensed with the ethanol production capacity of 2.25 Mt/a. As DMTE technology can turn the relatively abundant coal resources not food into ethanol, it can safeguard China's food supply while reduce air pollution.

Prof. Liu has published more than 430 research papers and got 600 authorized patents or more. He also received many awards in his scientific career, including The First Class of the National Technological Invention Awards (2014), The First Class of the National Scientific and Technological Progress Award (2017), Chinese Catalytic Achievement Award (2017), AIChE Professional Achievement Award for Innovations in Green Process Engineering (2018), Highest Science and Technology Awards of Liaoning Province (2019), etc.

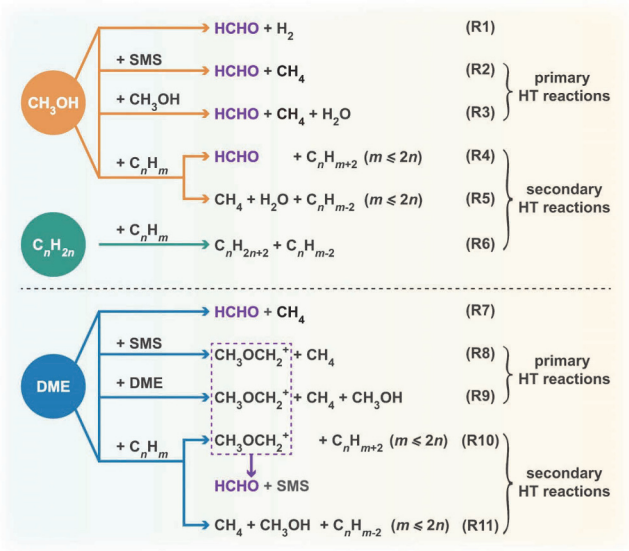

Scheme 1. Reaction pathways of HCHO generation and HT reactions involving methanol, DME, and alkenes.

photoionization MS to quantitatively detect HCHO in MTO at low-pressure. Despite these studies, quantitative detection of HCHO is still challenging, and particularly, the evolution of HCHO concentration during the entire MTO reaction, especially at the deactivation stage, has so far been lacking. In this context, it is challenging but imperative to quantitatively monitor HCHO in real time, which is the foundation for getting a full picture of complex reaction network of MTO, but also for achieving rational strategy for improving catalytic performance.

To tackle the aforementioned challenges, in this work, by the established colorimetric analysis method, the evolution of HCHO concentration throughout the MTO and DME-to-olefins (DTO) over SAPO-34 under real reaction conditions was *in situ* quantitatively determined. This allows us to further determining the H atoms trajectories throughout the reaction. On this basis, by combining theoretical calculation, *operando* spectroscopic analysis, isotope switch experiment and deactivation kinetics, the mechanism of HCHO generation at different stages of MTO and DTO is uncovered; the competition of HT and methylation reactions of methanol and DME, and its effect on the reaction network and catalyst deactivation are also revealed, which leads to the identification of deactivation models for MTO and DTO. The effect of cofeeding water and high-pressure H_2 on MTO reaction are investigated based on the direct experimental evidence from the quantitative detection of HCHO. Based on these understandings, DTO reaction is conducted combining with high-pressure H_2 cofeeding to further modulate the dynamic reaction network for the achievement of more moderate autocatalysis evolution.

2. Experimental

2.1. Catalyst and characterizations

SAPO-34 were synthesized following the procedure described in our previous work [37]. The H-form SAPO-34 were obtained by calcining the crystallized products at 873 K in air for 6 h to remove the template.

Elemental composition of the samples were determined from the quantitative elemental analysis of bulk composition obtained using a Philips Magix-601 X-ray fluorescence (XRF) spectrometer.

Powder X-ray diffraction (XRD) patterns of samples were recorded on a PANalytical X'Pert PRO X-ray diffractometer equipped with Cu K_α radiation (λ = 1.54059 Å), operating at 40 mA and 40 kV, scanning the 2θ angle from 5° to 60° with a scan rate of 5°/min.

The crystal morphology and average crystallite size were characterized by a Hitachi SU8020 Cold Field Emission scanning electron microscope (SEM).

Fourier Transform Infrared Spectroscopy (FTIR) study on NH_3 adsorption over H-form SAPO-34 was studied. The spectra were collected on a Bruker TENSOR27 spectrometer at a resolution of 4 cm^{-1} collecting 64 scans. H-form SAPO-34 samples were pressed into thin wafer (7.84 mg cm^{-2}) and *in situ* pre-treated in an IR cell under ultra-high vacuum at 723 K for 1 h prior to NH_3 adsorption. After the samples were cooled down to 303 K, NH_3 was introduced into the cell for 30 min, and then evacuated for 30 min to remove gaseous NH_3. Subsequently, the sample wafer was evacuated at 423 K for 30 min to remove the weakly adsorbed NH_3, and then cooled down to 303 K to record the spectrum.

2.2. Catalytic testing

For all MTO and DTO reactions, equimolar carbon amounts of methanol and DME were fed. The SAPO-34 catalyst powder was pressed and sieved into 40–60 mesh. Prior to reaction, the catalyst was activated under He flow at 723 K for 40 min, and then the temperature was readjusted to the reaction temperature.

All normal-pressure MTO and DTO reactions were carried out in a fixed-bed quartz tube reactor with an inner diameter of 4 mm under atmospheric pressure. Typically, 100 mg SAPO-34 was used. Methanol (> 99.8%) was fed by passing nitrogen through a saturation evaporator kept at 287.2 K. Gaseous DME (4.5 mol% dilution with helium) was directly fed at atmospheric pressure. In co-feeding experiments, H_2O (ultra-pure grade water) was fed by passing nitrogen through a saturation evaporator kept at 305 K, achieving equal relative partial pressure to DME (4.5%) and half of methanol (9%), and correspondingly, equal flow rate of N_2 was fed to achieve same contact time and partial pressure of C1 reactant for all co-feeding experiments. Differently, activity tests were conducted at varied contact time (0.004–0.596 g_{cat} h mol^{-1}). 5–100 mg SAPO-34 catalysts were diluted with 238–0 mg quartz sand (40–60 mesh) to keep the same bed volume. CH_3OH kept at 300.2 K and DME (9 mol% dilution with helium) were used.

All high-pressure MTO and DTO reactions were carried out in a fixed-bed stainless steel reactor lined with a quart tube with an inner diameter of 8 mm. Methanol (> 99.8%) was fed by a pump and vaporized in the lined quartz tube reactor. Typically, 250 mg SAPO-34 was used, the total pressure is 2 MPa,

and methanol weight hourly space velocity (WHSV) is 4.0 h^{-1}. Gaseous DME (mixed gas: 6.25 mol% DME, 6.25 mol% N_2, 87.5 mol% H_2) was fed with equimolar carbon amounts of methanol. Gas hourly space velocity (GHSV) is 11206.4 h^{-1}. For all reactions, a certain flow of N_2 was used as equilibrium gas to ensure that the partial pressure of C1 reactant and the contact time for each comparative experiment were identical.

Gaseous reaction products were kept at 473 K to avoid condensation and analyzed *via* online gas chromatography-mass spectrometer (GC-MS, Agilent 7890B/5977A) equipped with a PoraPLOT Q capillary column and a flame ionization detector. The conversion and selectivity of MTO and DTO reactions were calculated on a CH_2 basis. Both methanol and DME were considered as reactants in the calculation.

2.3. Operando DRIFT measurements

For *operando* diffuse reflectance infrared Fourier transform spectroscopy (DRIFT) experiments, the evolution of catalyst surface species as well as the gaseous products were simultaneously monitored by using an *operando* approach combining DRIFT spectroscopy with online MS (Pfeiffer Omnistar GSD 301 T3). DRIFT spectra and MS signal were simultaneously collected at 623 K with reaction proceeding.

DRIFT spectra were collected on a Bruker Tensor 27 instrument with a diffuse reflectance infrared cell with ZnSe window and a liquid nitrogen cooled Hg-Cd-Te detector. Before the measurements, 20 mg catalysts powder was loaded in the cell and flatten the surface, then pre-treated under a He flow at 773 K for 60 min and, subsequently, decreased to the reaction temperature of 623 K. CH_3OH was fed by passing 25 mL min^{-1} nitrogen through a saturator evaporator kept at 287.15 K. DME (4.5 mol% dilution with helium) at 27.5 mL min^{-1} was fed at atmospheric pressure to give the same CH_2-based WHSV as CH_3OH. Once the reactants were continuously introduced into the cell loaded with catalysts, the absorbance spectra were collected immediately by averaging 16 scans at 4 cm^{-1} resolution.

According to the database of the National Institute of Standards and Technology (NIST), the m/z values of the corresponding substances were referred as follow: Methanol (31, after subtracting the fragment ion signal of m/z = 31 from DME), DME (45), ethylene (26, after subtracting the fragment ion signal of m/z = 26 from propene), propene (41, after subtracting the fragment ion signal of m/z 41 from DME).

2.4. Ex situ solid-state NMR experiments

When the reaction of ^{13}C-CH_3OH (kept at 287.15 K with relative partial pressure of 0.09) or ^{13}C-DME (4.5 mol% dilution with helium) conversion was proceeded for a predetermined time (following the procedure mentioned in catalytic testing), reactants flow was cut off and the reactor was quenched by liquid nitrogen immediately. Then, the cooled catalysts were rapidly transferred into 4 mm magic angle spinning (MAS) NMR rotors in a glove box for solid-state NMR measurement. The solid-state NMR measurements were performed on a Bruker AvanceIII 600 spectrometer equipped with a 14.1 T wide-bore magnet using a 4 mm WVT MAS probe. The resonance frequencies for ^{13}C and ^{1}H nucleus were 150.9 and 600.13 MHz, respectively. The 1D ^{1}H-^{13}C cross-polarization (CP) spectra were recorded with a MAS frequency of 12 kHz. A 3400 scans were accumulated with the $\pi/2$ pulse length of 5.0 us for ^{1}H and 4.8 us for ^{13}C, a cross-polarization contact time of 3 ms and a recycle delay of 2 s. Referencing chemical shifts were to adamantane with the upfield methine peak at 29.5 ppm. The spectra were recorded at room temperature.

2.5. $^{12}C/^{13}C$ switch experiments

The $^{12}C/^{13}C$ methanol and $^{12}C/^{13}C$ DME switch experiments were conducted at 573 K over SAPO-34, and all reactants were fed in following the procedures described in catalytic testing. Firstly, building up ^{12}C hydrocarbon pool in HSAPO-34 by feeding ^{12}C-methanol or ^{12}C-DME for 18 min. Then the feeding of ^{12}C-methanol or ^{12}C-DME was stopped and ^{13}C-methanol or ^{13}C-DME was switched into the reactor for 0.5, 1.0, and 1.5 min, respectively, and following closely, the reactants flow was cut off and the reactor was quenched by liquid nitrogen immediately. The isotopic distributions of gas effluent products and retained material confined in the catalyst (following the procedure in coke analysis) were analyzed *via* GC-MS (Agilent 7890B/5977A).

2.6. Coke analysis

The total coke amounts of the spent catalysts were determined by thermogravimetric analysis (TGA) performed on a TA SDTQ 600 analyzer. Typically, about 10 mg sample was loaded and heated from room temperature to 1173 K with a temperature-programmed rate of 10 K min^{-1} under an air flow of 100 mL min^{-1}. The weight loss below 523 K is ascribed to water desorption.

20 mg spent catalysts were dissolved in 0.4 mL 20% hydrofluoric acid (HF) solution in a Teflon vial to liberate the retained species, and then it was extracted by the addition of 0.5 mL dichloromethane (CH_2Cl_2) containing hexachloroethane (C_2Cl_6) as internal standard. The CH_2Cl_2-extracted organic phase, hereinafter called "soluble coke" (molecular weight smaller than 300 g mol^{-1}), was analyzed by GC-MS (Agilent 7890A/5975C) equipped with a HP-5 capillary column and identified by reference to the mass spectral library of NIST08.

2.7. Theoretical calculations

DFT calculations performed with the Gaussian 09 package [38] were applied to calculate the reaction energy barriers of methylation reactions. An extended 74T($SiP_{36}Al_{37}O_{119}H_{59}$) cluster model extracted from the crystallographic CHA structure (from the International Zeolite Association) was used to represent SAPO-34 and the locations of BAS were chosen at the 8-MR window, accessible for adsorbents and surrounded by maximum reaction space [39]. The ωB97XD hybrid density function with 6-31G(d,p) basis sets and semi-empirical AM1

were employed to predict the geometries of various adsorption structures and transition states. ωB97XD, a hybrid meta method, can describe empirical dispersion and long-range dispersion interactions [40]. During the structure optimizations, the 8-MR window, $(SiO)_3$-Si-OH-Al-$(SiO)_3$ active center and the adsorbed species were optimized using the ωB97XD method in the high level layer, while the rest of atoms were set in the low-level layer with semi-empirical AM1 method. All the atoms apart from the terminal H atoms were relax during the whole structure optimization. To obtain highly accurate energies, the single point energies were calculated at the level of ωB97XD/6-31G(d,p) based on the optimized structures. The frequency calculations were performed at the same level as geometry optimizations. The transition state had only a single imaginary frequency, and the adsorbed state was located at the energy minima of the potential energy surface without imaginary frequencies. The intrinsic free energies barriers ($\Delta G^{\ddagger}$) under the real reaction condition at 623 K for each elementary reaction was obtained from the ωB97XD/6-31G(d,p) total electronic energies and the thermal correction from the ωB97XD/6-31G(d,p): AM1 frequency calculations. The energies reported here have been corrected for zero-point vibration energies.

3. Results and discussion

3.1. HCHO detection and formation mechanism in different reaction stages of MTO reaction

3.1.1. General feature of MTO reaction

The characterization results of SAPO-34 are shown in Figs. S1–S3. SAPO-34 exhibits a Si/(Si + Al + P) ratio of 0.085. The XRD pattern shows the characteristic CHA structure with a high crystallinity and indicates no observable impurity phases present (Fig. S1). SEM demonstrates its cubic crystal morphology and average crystallite size of about 8 μm (Fig. S2). FTIR spectra of NH_3 adsorption (Fig. S3) proves that almost no Lewis acid sites (LASs) are present on SAPO-34 used in this work, and the reaction is almost performed based on Brönsted acidic sites (BASs).

The methanol conversion over SAPO-34 at 623 K follows the characteristic inverse S-shape curve with time on stream (Fig. 1(a)), with a period of full conversion followed by a rapid decline in conversion after reactants (methanol and/or DME) breakthrough, which is the typical behavior of MTO and irrespective of catalyst topology [41]. This conversion curve, serving as the "open-line" of MTO reaction, reflects the three successive reaction stages, including induction stage (too short to be observed in this work), *pseudo* steady-state stage and deactivation stage. The formation of HCHO in MTO has been noticed [8,12,16,24,34,35], but was often focused on the initial stage and/or under low conversion conditions.

3.1.2. Colorimetric analysis method of HCHO quantitative detection

Here, we adopt a colorimetric analysis method to quantify HCHO during the entire MTO and DTO process. First, the reaction effluent is condensed into a centrifuge tube placed at the outlet end of the fixed-bed reactor for a predetermined time, 5 min typically. Subsequently, HCHO was quantified by the following chromogenic reaction (Scheme 2 [42]).

After 8 min of chromogenic reaction, take pictures to record the color of the solution. If the color changed from colorless to purple-red, the existence of HCHO could be confirmed, and the depth of the purple-red is proportional to the content of HCHO. Based on a series of chromogenic reaction for HCHO solutions with different concentrations, the quantitative relationship between HCHO concentration and color of chromogenic reaction was obtained (Fig. S4, same as Figs. 1(c), 4(c), 8 and 9).

Several representative oxygenates, some of which have been identified or speculated during the MTO reaction, including aldehydes (HCHO, CH_3CHO, CH_3CH_2CHO), alcohols (CH_3OH, CH_3CH_2OH), acids (HCOOH, CH_3COOH), ketones (CH_3COCH_3) and esters ($HCOOCH_3$, CH_3COOCH_3), were selected for comparative experiments. All representative oxygenated compounds are colorless in colorimetric determination (Fig. S5) except for HCHO, which is purple. These results indicate that the above oxygenated compounds do not interfere with the chromogenic analysis of HCHO in the MTO/DTO reaction.

Furthermore, blank experiments for HCHO detection on the fixed-bed reaction device system were conducted. The results in Fig. S6 shown that almost no HCHO was detected during the conversion of methanol and DME in the empty reaction device system under reaction conditions in this work. These results deliver the evidence of the reliability and effectiveness of this method, and enable us to conduct quantitative analysis of HCHO in the MTO/DTO reaction.

3.1.3. The evolution of HCHO concentration and zeolite surface species in MTO reaction

As shown in Fig. 1(c), a trace concentration of HCHO was detected at the initial stage, and HCHO concentration faded away when methanol was completely converted, and then increased considerably during the deactivation stage, especially when the conversion was lower than 50%. These results, for the first time, directly establish the evolution of *in situ* generated HCHO concentration as the reaction proceeds from onset to decay. Based on this, we next investigate the mechanism of HCHO formation at each stage of MTO, by determining the H atoms trajectories, tracking the dynamic catalyst surface, and evaluating the thermodynamic feasibility of correlative HT reactions.

The *operando* approach–combing DRIFT spectra and MS–was employed to track the dynamic catalyst surface (Fig.

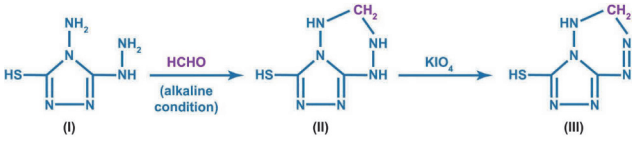

Scheme 2. Chromogenic reaction for HCHO detection [42]. HCHO condenses with 4-amino-3-hydrazino-5-mercapto-1,2,4-triazole (AHMT, compound I) under alkaline conditions to form compound II, which are then oxidized by potassium periodate to purple-red 6-mercapto-5-triazole (4,3-b)-S-tetrazine (compound III).

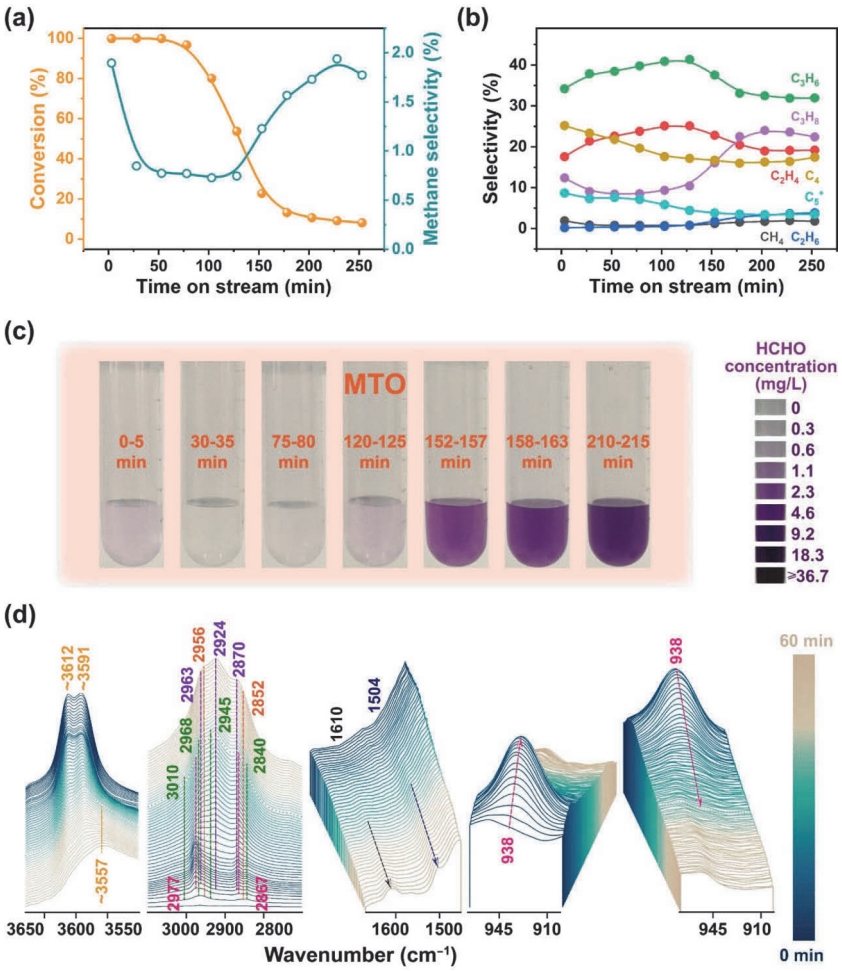

Fig. 1. Conversion and methane selectivity (a), product distribution (b), and colorimetric determination of HCHO concentration (c) versus time on stream for MTO reaction over SAPO-34 at 623 K with a methanol WHSV of 2.0 h^{-1}; (d) *Operando* DRIFT spectra recorded during methanol conversion on SAPO-34 at 623 K from 0 to 60 min.

1(d)) and effluent species profiles (Fig. S7) during methanol conversion. Upon adsorption of methanol (2956 and 2852 cm^{-1}) [43,44], with the gradual disappearance of Brönsted acid sites (BASs, 3612 and 3591 cm^{-1}) [45], DME (3010, 2968, 2945 and 2840 cm^{-1}) [43,44] and surface methoxy species (SMS, 2977, 2867 and 938 cm^{-1}) [43,44,46] were instantly formed. The intensity of SMS increased from 0 to 4.3 min, and then gradually diminished and vanished after ~15 min during initial stage. Concurrently, dimethylcyclopentenyl cationic (1504 cm^{-1}) [47,48] and aromatic species (1610 cm^{-1}) [46,49] appeared and increased in intensity with reaction proceeding, and simultaneously, a broad band centered at 3557 cm^{-1} appeared, attributed to the Si(OH)Al groups interacting with the confined organic species as adsorbates. Real-time DRIFT spectra clearly demonstrate the dynamic evolution of zeolite surface species with the proceeding of reaction, from BASs to the SMS and to multi-carbon species with higher H-unsaturation, which is originated from the successive occurrence of HT reactions. This eventually contributes to the dynamically evolving molecular routes of the MTO.

3.1.4. The mechanism of HCHO generation at the initial stage of MTO reaction

The aforementioned evolution trend of HCHO concentration exhibited similar time-resolved variations with CH_4 selectivity (Fig. 1(a)), suggesting that they originate from the same pathway. During the initial stage, the active sites relay from BASs to the SMS (Fig. 1(d)), and SMS could abstract a hydride from methanol, stoichiometrically generating a molecule of CH_4 and HCHO. This elementary reaction has been assessed by theoretical calculations [17,21,50–52], giving the energy barrier of 147–171 kJ mol^{-1} [21,50–52] and $\Delta G^{\ddagger}$ of 222 kJ mol^{-1} [17]. We also performed DFT calculation for this HT reaction at 623 K over SAPO-34, giving the $\Delta G^{\ddagger}$ of 200 kJ mol^{-1} (Fig. 2(a)). However, it is crucial to take the first step into account, i.e., the SMS formation by eliminating a water molecule from adsorbed methanol ($\Delta G^{\ddagger}$ is 173 kJ mol^{-1} [53]). The above HT reaction between SMS and methanol was further assessed using a molecule of produced water as an assisted molecule, and a lower $\Delta G^{\ddagger}$ of 164 kJ mol^{-1} was obtained, due to a more stable transition state stabilized by water (Fig. 2(b)). Similar result was reported by Hu and coworkers [54]. In addition to the stepwise HT mechanism, the concerted HT mechanism between two methanol molecules was also calculated with $\Delta G^{\ddagger}$ of 176 kJ mol^{-1} (Fig. 2(c)). These results suggest that HT from methanol to the SMS assisted by water, is the main route for the for-

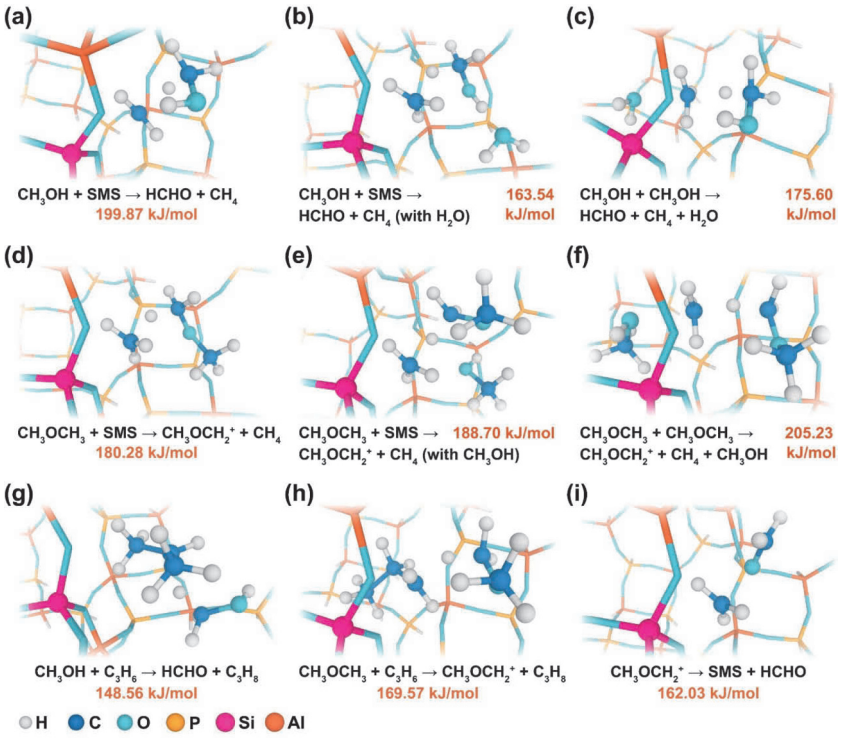

Fig. 2. Optimized transition states structures and free energies barriers ($\Delta G^{\ddagger}$) of HT reactions over SAPO-34 at 623 K.

mation of CH_4 and HCHO at the very beginning of MTO.

3.1.5. The mechanism of HCHO generation at the deactivation stage of MTO reaction

Interestingly, during the deactivation stage, CH_4 selectivity was close to that in the initial stage (Fig. 1(a)), but HCHO concentration was much higher (Fig. 1(c)), suggesting that there are other pathways contributing to HCHO generation. Noting that when the conversion was below 50%, alkanes (especially propane) selectivity increased apparently, accompanying with a decrease in alkenes (especially propene) selectivity (Fig. 1(b)). These observations allow the deduction that HT from methanol to alkenes giving HCHO and alkanes contributes significantly to the higher HCHO concentration after the occurrence of incomplete methanol conversion. It was further supported by the lower calculated $\Delta G^{\ddagger}$ of HT reaction for methanol with propene (as a representative of alkenes, Fig. 2(g), 149 kJ mol^{-1}) than that with SMS (Fig. 2(b), 164 kJ mol^{-1}). Nevertheless, from the perspective of the overall complex reaction network for methanol conversion (Fig. 3), it should be stated that HT reactions between olefinic species, i.e. OIHT [5–7], are the significant pathway to generate alkanes.

3.1.6. The reaction network of methanol to hydrocarbon process

As shown in Fig. 3, methanol conversion over zeolite is a dynamic process for C–C assembly from C1 reactant through direct and/or indirect mechanisms [1–4]. Correspondingly, open-line of MTO reaction is observed, reflecting the evolution of the domino likes [4] reaction sequence running from initiation to decay. Accompanying with the growth of the carbon chain, unsaturation degree of hydrocarbons, especially the retained organics in catalyst, also progressively increases (from olefin to polyene, cyclopentadiene, aromatics, and to polycyclic aromatic hydrocarbons (PAHs)). The increase in unsaturation degree of hydrocarbons is driven by the HT reaction—the "hidden-line" of MTO, in which HT from the H-donor (such as methanol, cyclic or chain alkane or alkene, and aromatics) to H-acceptor (frequently methanol and alkenes), resulting in the more H-deficient species (HCHO, polyenes and PAHs) and more saturated (cyclo)alkanes species (including methane), respectively [5–20,26,27]. Therefore, HT reaction not only generates unsaturated active intermediates for methanol conversion, but also is a pivotal step for the formation of carbon deposits, which plays a critical role in the initiating, sustaining, and decaying of MTO autocatalysis. Particularly, the role of HCHO in the reaction network is further involved in Prins reaction with olefins to give polyene, and in alkylation reaction with aromatics to give products mediated by benzyl carbenium ions [5,8,18–20,26,27] (Fig. 3), which assists the formation of the hydrocarbon pool (HCP) species in the initial stage and the generation of PAHs in the deactivation stage, ultimately accelerating both reaction initiation and deactivation.

3.1.7. The mechanism of HCHO generation at the pseudo steady-state stage of MTO reaction

Notably, almost no HCHO was detected at the *pseudo* steady-state stage, in which methanol was completely converted *via* the highly-efficient autocatalytic hypercyclic network, generating abundant alkenes as main effluent products and aromatics retained in zeolite, and thus, HT reactions mainly occur between these species, i.e. product-induced HT. The

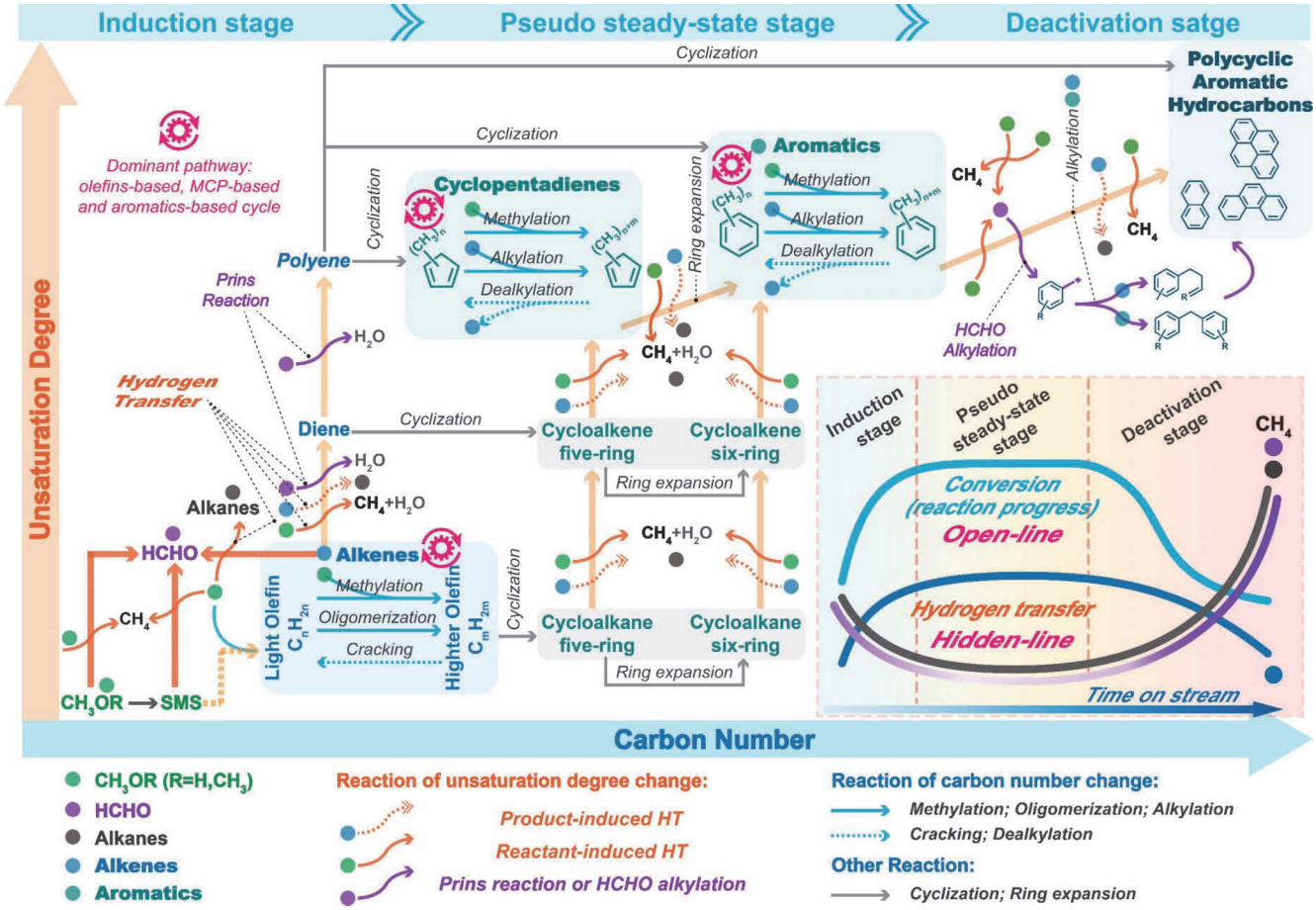

Fig. 3. The proposed dynamic reaction network of methanol to hydrocarbon process with hydrogen transfer reactions as hidden line.

above observations allow us to deduce the condition of HCHO generation–the high local concentration of reactant (methanol), where methanol is not full converted, i.e., the hypercycle for methanol conversion has not yet been established (induction stage) or has subsided (deactivation stage). This is further supported by Lercher *et al*. [5] who proposed that MIHT dominated the generation of HT products in MTO at partial conversions, whereas the contribution of OIHT is negligible owing to the inhibition of olefin adsorption at BASs by the presence of methanol, and OIHT is only relevant when full methanol conversion is achieved.

3.2. HCHO detection and formation mechanism in different reaction stages of DTO reaction

3.2.1. General feature and evolution of HCHO concentration for DTO reaction

As shown in Figs. 4(a)–(c), when using sole DME feed, the reactivity loss rate slowed down and the corresponding HCHO concentrations were also lower compared with sole methanol feed. These results allow us to argue the specific role of methanol on HCHO formation and catalyst deactivation, which, however, is markedly different from DME.

Notably, Olsbye et al. [18–20] proposed that HCHO can be formed exclusively from methanol, but not from DME. This view was also supported by Bhan *et al*. [26], who concluded that DME cannot undergo an analogous HT reaction like methanol because there exists no stable product of DME dehydrogenation. However, Lercher *et al*. [17] recently proposed that the reactivity of DME for the formation of CH_4 and HCHO is higher compared to methanol. Regardless of these controversies, in this work, HCHO was indeed detected in DTO, and, particularly, its concentration was far less than that in MTO (Fig. 4(c)). Such observation was more clearly confirmed by the reactions of MTO and DTO with similar initial conversion of 80% over SAPO-34 at 623 K (Fig. S8).

3.2.2. The mechanism of HCHO generation at the initial stage of DTO reaction

The evolving routes of dynamic catalyst surface (Fig. 4(c)) and effluent species profiles (Fig. S9) during DME conversion are analogous with MTO reaction, except that the evolution process in the initial stage is faster. During DTO reaction, the SMS emerged after DME adsorption and then gradually diminished (Fig. 4(c)), and moreover, trace amount of HCHO was detected together with high methane selectivity at the initial stage of DTO (Figs. 4(a), (c)). The elementary steps for HCHO generation from DME were studied by theoretical calculations. Firstly, adsorbed DME eliminates a methanol molecule to generate SMS ($\Delta G^{\ddagger}$ is 156 kJ mol^{-1} [53]). Then, SMS further reacts

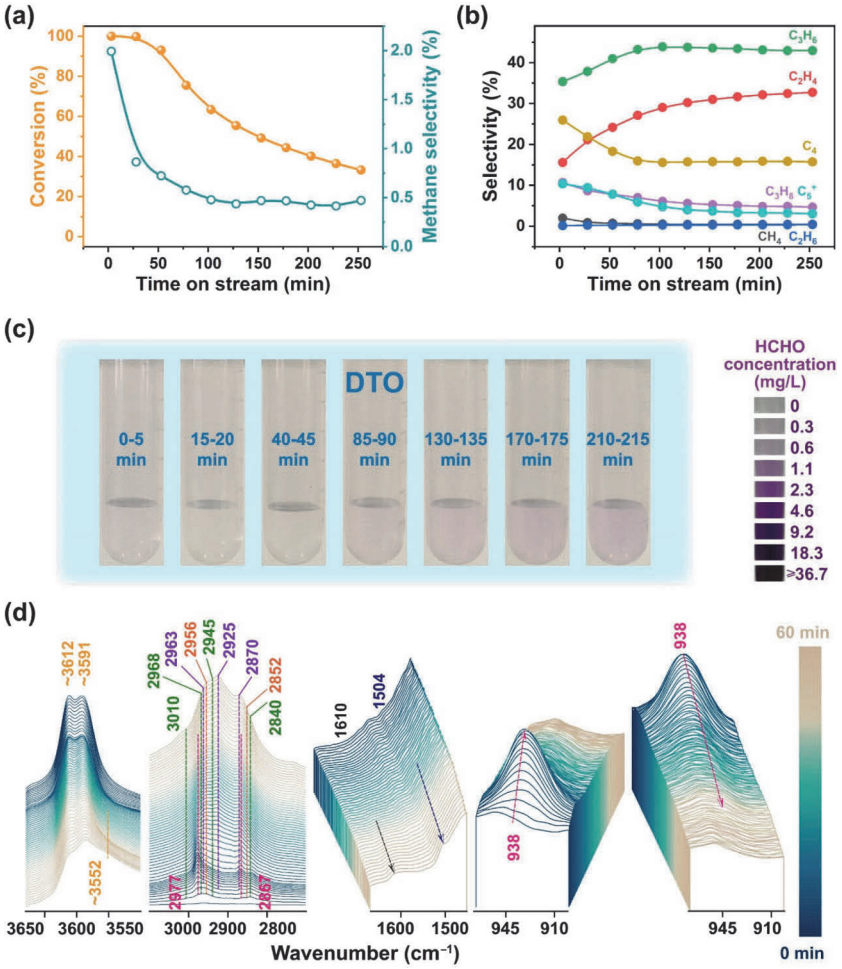

Fig. 4. Conversion and methane selectivity (a), product selectivity (b) and colorimetric determination of HCHO concentration (c) versus time on stream for DTO reaction over SAPO-34 at 623 K with a DME WHSV of 1.4 h^{-1}, achieving the same CH_2-based WHSV of 6.2 × 10^{-3} mol_{CH2} h^{-1} g_{cat}^{-1} as MTO in Fig. 1(a). (d) *Operando* DRIFT spectra recorded during DME conversion on SAPO-34 at 623 K from 0 to 60 min.

with another DME molecule assisted with a methanol molecule generated by the first step to form CH_4 and methoxymethylene carbenium ion ($CH_3OCH_2^+$) giving a $\Delta G^{\ddagger}$ of 189 kJ mol^{-1} (Fig. 2(e)), and $\Delta G^{\ddagger}$ is 180 kJ mol^{-1} without assisting molecule (Fig. 2(d)). Subsequently, the unstable $CH_3OCH_2^+$ dissociates into SMS and HCHO ($\Delta G^{\ddagger}$ is 162 kJ mol^{-1}, Fig. 2(i)). The concerted HT mechanism between two DME molecules was also evaluated, giving a higher $\Delta G^{\ddagger}$ of 205 kJ mol^{-1} (Fig. 2(f)).

3.2.3. The mechanism of HCHO generation at the deactivation stage of DTO reaction

Notably, the significantly increased alkane selectivity and concomitantly decreased alkene selectivity at deactivation stage of MTO (Fig. 1(b)) were not observed in DTO (Fig. 4(b)), and the propane/propylene ratio, which is often considered to be an HT index, for MTO reaction is higher than DTO reaction, especially at the deactivation stage (Fig. S10). This inspired us to evaluate the HT reaction of DME with alkenes. Taking HT reaction of DME with propene (as a representative of alkenes) to produce propane and $CH_3OCH_2^+$ as an example, the calculated $\Delta G^{\ddagger}$ was 170 kJ mol^{-1} (Fig. 2(h)). The $\Delta G^{\ddagger}$ of HT reaction using DME as a H-donor to form HCHO is higher than methanol for both the SMS (25 kJ mol^{-1}) and propene (21 kJ mol^{-1}), which provide theoretical evidence for the lower HCHO concentration during the DTO reaction. Moreover, the $\Delta G^{\ddagger}$ of HT reaction with propene is 15 and 18 kJ mol^{-1} lower than with SMS for methanol and DME, respectively, supporting the higher HCHO concentration at deactivation stage than initial stage for both MTO and DTO.

Interestingly, unlike MTO reaction, the methane selectivity does not increase significantly and remains at a low level during the deactivation stage of DTO (Fig. 4(a)), even at very low conversion level (Fig. S11). Consensus on the mechanism for methane generation after the induction stage of MTO is the result of HT reaction using methanol as H-acceptor, accepting hydrogen from the H-donor, such as (a)cyclic-alkane/alkene, aromatic and coke (Fig. 3) [26]. Accordingly, this observation suggests that using DME as a H-acceptor (Scheme 1, R11) is difficult to occur these HT reactions for methane generation (Scheme 1, R5). Comprehensively, these experimental and computational results provide conclusive evidence for the strong HT ability of methanol compared to DME, whether as H-donor (generation of HCHO) or acceptor (generation of CH_4).

3.2.4. The contribution of methanol HT to HCHO generation in DTO reaction

Actually, we can hardly exclude the contribution of methanol HT to the generation of HCHO in DTO, because methanol is inevitably produced during the conversion of DME, and the key may lie in the concentration of methanol in the reaction system, which is related to the thermodynamic equilibrium between CH_3OH and DME. By comparing the experimental molar fraction of CH_3OH and DME in the effluent with that estimated in the thermodynamic equilibrium state at different conversions (see Supplementary Note for detailed calculation), it can be observed that for all MTO and DTO reactions with initial conversion of 100% (Figs. 1(a) and 4(a)) and 80% (Fig. S8), the traditionally-viewed CH_3OH-DME equilibrium was not established (Fig. 5). Actually, the reactant concentration in the reactor was closer to the feed composition, i.e. dominating by CH_3OH in MTO, and by DME in DTO, where only a small amount of methanol was produced. More importantly, the methanol molar fraction in MTO reaction with initial conversion of 80% was higher than that when methanol was initially full converted (Fig. 5(a)), corresponding to its higher HCHO concentration (Figs. 1(c) and S8). The same results were also observed in the DTO reaction (Fig. 5(b), Figs. 4(c) and S8). These observations present a positive correlation between methanol concentration and HCHO concentration. More importantly, it also allows us to argue that HCHO in DME conversion process is likely to generate from its product of methanol, but we can hardly exclude the routs form DME directly, although theoretical calculations give higher energy barriers.

3.3. Competitive propene methylation and hydrogen transfer with methanol and DME

C1 reactant undergo competitive HT and methylation reactions with HCP species (Fig. 3). We next explore such competition and its effect on reaction network by assessing the HT and methylation ability of methanol and DME to HCP species, taking propene as an example. As shown in Figs. 6(a) and (b), the differences for overall free energy barriers between methylation and HT reactions with propene were found to be 9 kJ mol^{-1} for methanol (139 kJ mol^{-1} [53] and 149 kJ mol^{-1}) and 33 kJ mol^{-1} for DME (136 kJ mol^{-1} [53] and 170 kJ mol^{-1}). This indicates that the methylation and HT reactions of methanol are clearly in competition in MTO, and instead, the higher overall barrier makes HT of DME less efficient in DTO.

Next, the impact of above competition on the reaction network was assessed. Firstly, MTO and DTO reactions were observed to share the same retained active intermediates, i.e., heptamethylbenzenium cation and pentamethylcyclopentenyl cation, captured by *ex situ* ^{13}C CP/MAS NMR after 15 min of reaction (Fig. S13). Further, $^{12}C/^{13}C$ isotope switching experiments were conducted to distinguish the mechanistic routes of methanol and DME conversions (Figs. 6(c) and (d)). Hexamethylbenzene (hexaMB), with the highest ^{13}C incorporation among the confined organics, was identified as the most reactive aromatic species, in line with previous work [55,56]. For MTO, the comparable ^{13}C incorporation between hexaMB and effluent olefins implies the prevalence of aromatics-based cycle. While for DTO, the much higher ^{13}C incorporation for olefins than hexaMB and other aromatics signifies the operation of both aromatics- and olefins-based cycles [57,58]. Moreover, the higher reactivity of methanol for HT reaction than DME is beneficial to the generation of H-deficient products (generating from HT reaction of methanol directly or indirectly (*via* HCHO)), especially including the highly reactive aromatic species, thus also making aromatics-based cycle more predominant in MTO (Fig. 6(e)). In addition, although the product water in MTO is twice that of DTO under the above reaction conditions (full conversion), the prevailing aromatics-based cycle in MTO suggests that the strong HT ability of methanol is less affected by product water in this work, although water is generally considered to be an inhibitor for HT reaction [59,60].

We have shown that the competition of methylation and HT is different for methanol and DME and it will affect the relative extent of the alkene and arene cycles. In addition to this, the competition of these two pathways for both methanol and DME changes with the progress of the reaction. The reaction barrier for methylation of alkenes and aromatics by methylating reagents (methanol, DME, or SMS) drops continuously with increasing number of carbon atoms of alkenes [55,61–67] and

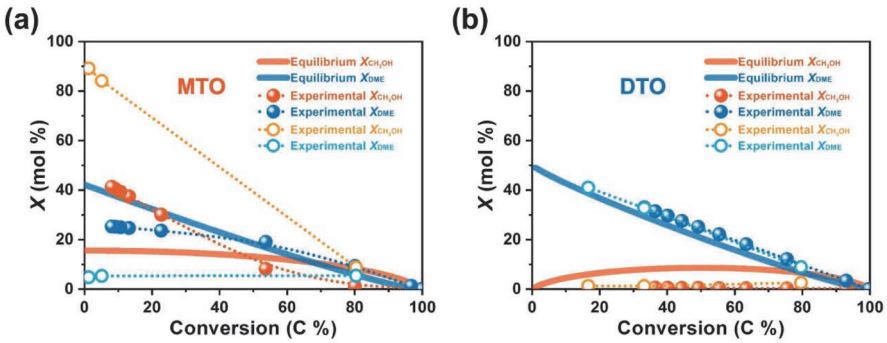

Fig. 5. The experimental and calculated molar fraction of CH_3OH and DME as a function of conversion for MTO (a) and DTO (b) reactions, over SAPO-34 at 623 K. Solid lines: calculated thermodynamic equilibrium molar fraction of CH_3OH (orange) and DME (blue) according to the assumption that the CH_3OH-DME equilibrium is always established. The detailed calculations are referred to Ref. [19] and described in supporting information and Fig. S12. Dashed lines: experimental molar fraction of CH_3OH (orange and yellow) and DME (blue and light blue) in the effluent. Dashed lines with orange and blue ball: MTO and DTO reactions with an initial conversion of 100%, reaction conditions are same as Figs. 1(a) and 4(a). Dashed lines with yellow and light blue circle: MTO and DTO reactions with an initial conversion of 80%, reaction conditions are same as Fig. S8.

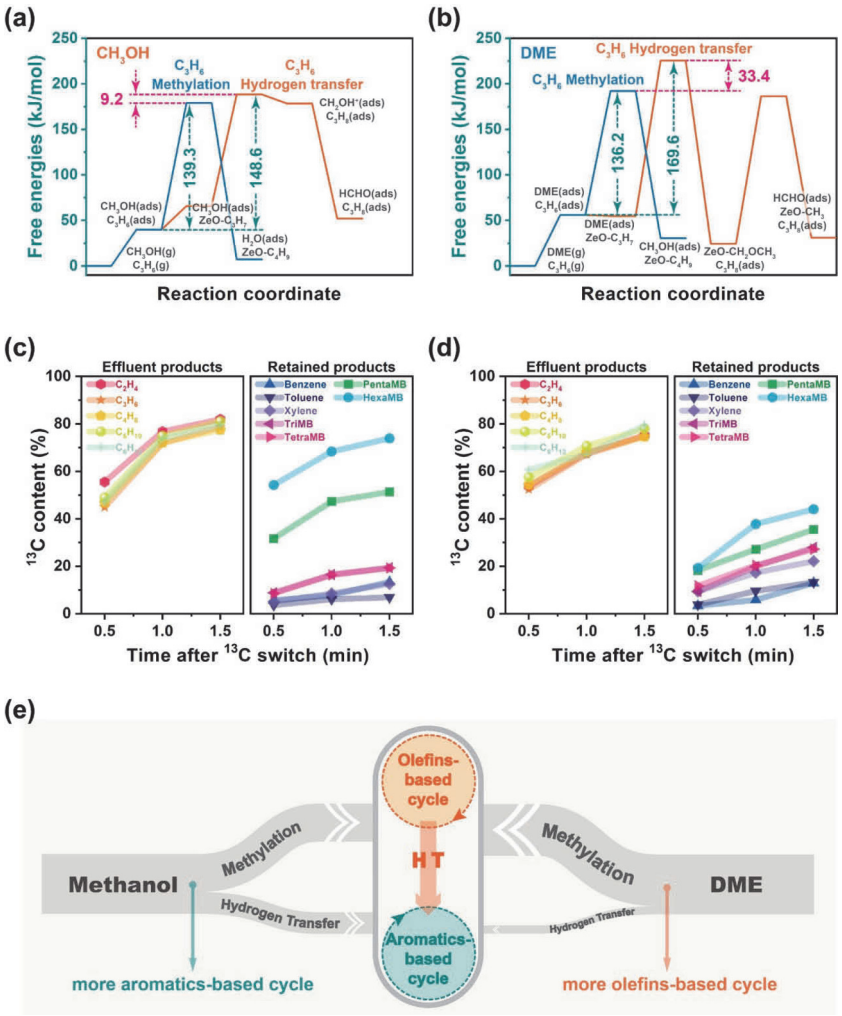

Fig. 6. Free energy profiles of propene methylation and HT reactions with methanol (a) and DME (b) over BASs of SAPO-34 at 623 K. Time evolution of ^{13}C content in effluent olefins and retained aromatics formed in the $^{12}C/^{13}C$ methanol (c) and $^{12}C/^{13}C$ DME (d) switching experiments over SAPO-34 at 623 K with ^{12}C-methanol/DME feeding for 18 min followed by 0.5, 1.0, and 1.5 min of ^{13}C-methanol/DME feeding, respectively. Reaction conditions are same as Figs. 1(a) and 4(a). (e) Proposed predominant reaction pathways of methanol and DME conversions.

methyl group substituents on the aromatic ring [65,68], respectively. Therefore, during the dynamic C–C assembly process, the methylation reaction is increasingly favorable and dominant at the *pseudo* steady-state stage. While, higher reactant concentration under semi-conversion conditions, i.e., initial and deactivation stages where the hypercyclic network does not operated efficiently, is favorable for reactant HT reactions.

3.4. Deactivation mechanism of MTO and DTO reactions

Based on the understanding of the competition between HT and methylation reactions of methanol and DME, and the mechanism of HCHO generation, we investigate next their effects on deactivation mechanism by using a deactivation model. The deactivation model considers that deactivation is a coking process driving by reactants and/or products, in which three kinds of reactions are considered [69]: reactants (R) to effluent products (P), products and reactants to coke (C), with corresponding rate constants of k_1, k_2, and k_3, respectively (Fig. 7(a)). Therefore, the reaction system can be described by the following model[69] (assuming the initial conversion is 100%):

$$R \xrightarrow{k_1} P \quad -d[R]/dt = (k_1 + k_2) \times N \times [R] \tag{1}$$

$$R \xrightarrow{k_2} C \quad d[C]_i/dt = (k_2 \times [R] + k_3 \times [P]) \times [N]_i \tag{2}$$

$$P \xrightarrow{k_3} C \quad d[P]/dt = (k_1 \times [R] - k_3 \times [P]) \times \mathrm{N} \tag{3}$$

where N is the number of active sites. For simplicity, all reactions are assumed to be first order to the reactant. The reactor was modelled as a series of 10 segments, where each segment was considered a perfectly mixed sub-reactor. The concentrations of R, P and C were integrated along the reactor (10 segments) for each reaction time, moreover C and N in each reactor segment (i) were integrated with reaction time (j):

$$N_{ij} = N_{i,j-1} - C_{i,j} \tag{4}$$

Using the model of catalyst deactivation (Eqs. (1)–(4)) [69] to fit the reaction results (reactant conversion versus time on stream), the corresponding rate constants k_1, k_2 and k_3 can be obtained (Fig. 7(b)). The kinetic parameters have been esti-

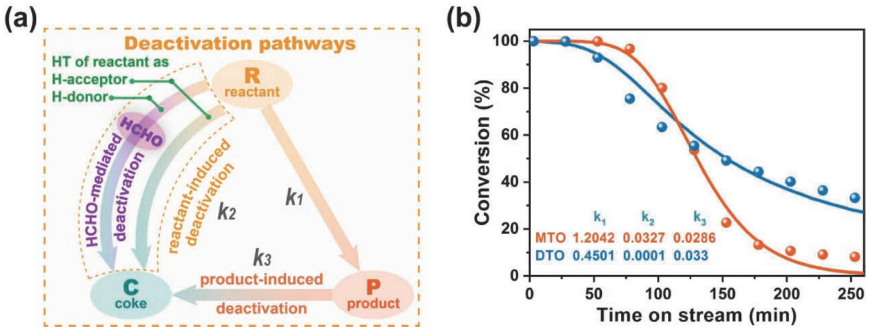

Fig. 7. (a) The principal catalyst deactivation pathways for methanol and DME conversion. (b) The conversion with time on stream for MTO and DTO reactions over SAPO-34 at 623 K. Points: experimental results, reaction conditions are same as Figs. 1(a) and 4(a); Solid lines: the fitted lines according to the deactivation model (Eqs. (1)–(4)).

mated by the trust-region-reflective algorithm (default algorithm for *lsqnonlin* function in MATLAB) and the differential equations have been solved by the *ode23s* function in MATLAB, which is based on a modified Rosenbrock formula of order 2. Optimization of the kinetic parameters was performed by minimizing the error objective function (Eq. (5)), which is the difference between the experimental and calculated values of the reactant conversions in MTO and DTO reactions.

$$EOF = \sum_{i=1}^{n_{exp}} (X_{i(exp)} - X_{i(cal)})^2 \quad (5)$$

where, $X_{i(exp)}$ and $X_{i(cal)}$ are the experimental and calculated values at experimental point *i*.

For MTO, the comparable values of k_2 and k_3 means a typical mixed reactant/product-induced deactivation process, corresponding to the proposed layer-by-layer inhomogeneous "cigar burn" model [70,71]. However, the relative value of kinetic constant obtained for reactant-induced coke formation (k_2) is much smaller than that for product-induced coke formation (k_3) in DTO, which is consistent with its relatively homogenous deactivation process.

The deactivation kinetic results reveal that methanol has a direct and significant contribution to catalyst deactivation. The nature of deactivation is a coking process with the decay of active aromatic species into on-surface or in-pore inactive and irreversibly adsorbed PAHs, which is driven by HT reaction. The identified HT pathways include conventional OIHT and reactant-induced HT, which respectively drive the product- and reactant-induced deactivation process. Originating the strong HT ability of methanol both as H-acceptor (production of methane and H-poor species directly promoting coking process) and H-donor (production of HCHO triggering HCHO-mediated deactivation process [5,8,18–20,26,27], Fig. 3), reactant-induced deactivation is critical for MTO. Differently, the higher overall barrier of HT reactions for DME with weak HT ability, depresses the reactant-induced HT reactions and thus the generation of HCHO and alkanes in DTO. This was further evidenced by the lower relative content of insoluble coke and higher relative content of polymethylbenzene based on coke analysis by TG and GC-MS experiments (Fig. S14). Therefore, using DME as feedstock could largely depress the reactant HT reactions, and thus reactant-induced deactivation is marginalized and a moderate deactivation mode could be achieved, mainly relevant with the product-induced deactivation. In addition, the constrained mass transfer of DME relative to methanol over SAPO-34 alleviates the high local chemical potential of reactant by attenuating its local enrichment, thereby generating relatively moderate reaction kinetic [53]. Comprehensively, originating from the weak HT ability and frustrated mass transfer of DME, the DTO reaction is characterized by moderate and homogenous reaction and deactivation.

3.5. Strategies for mitigating catalyst deactivation

The above uncovered deactivation mechanism provides fundamental basis for mitigating catalyst deactivation. Strategies to circumvent deactivation could be conceptually achieved by mitigating coking process corresponding to k_2 and k_3 (Fig. 7(a)), which can be realized by inhibiting the reactant- and product-induced HT reactions through minimizing their chemical potential. Obviously, this can be realized directly *via* the strategy supported by the substantive evidence in this work–minimizing methanol chemical potential through replacing methanol (higher HT ability) with DME (higher methylation ability), for which it inhibits the methanol involved HT reactions, especially including the generation of HCHO. Cofeeding water [59,72–74] and high-pressure H_2 [30,75,76] in MTO have been reported to extend catalyst lifetime and mitigate catalyst deactivation. Notably, Bhan *et al.* [26,28–31] proposed that the above strategies can scavenge the generated HCHO by hydrolysis and hydrogenation, rationalizing their effect on MTO. However, direct experimental evidence is still lacking. As such, we next revisit the two strategies from the perspective of HCHO, based on the direct experimental evidence from the quantitative detection of HCHO.

3.5.1. The effect of H_2O cofeeding on MTO reaction

As shown in Fig. 8(a), cofeeding with appropriate amounts of water to methanol feed over SAPO-34 at 723 K prolongs the catalyst lifetime, in line with previous work [73,75,77]. Additionally, the induction period of MTO (performed at 548 K to observe induction stage) is extended by cofeeding water and increases with increasing the partial pressure of water in the feed (Fig. 8(d)), which is consistent with the observations by Weckhuysen *at al.* [59] Correspondingly, the quantification of HCHO was conducted. A considerable quantity of HCHO was

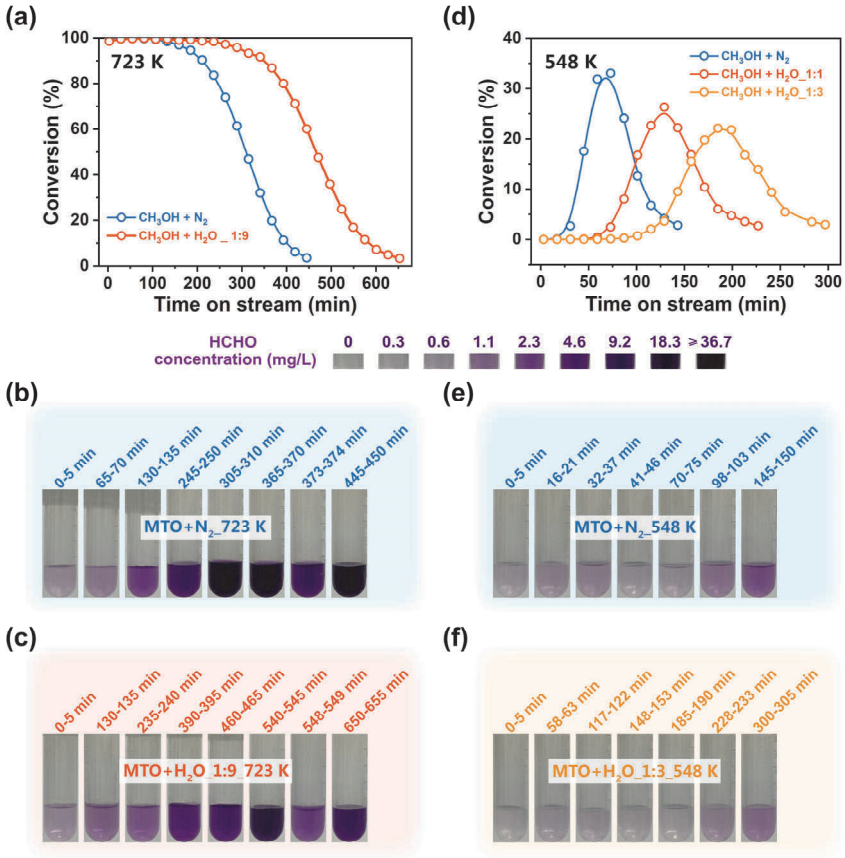

Fig. 8. Cofeeding H_2O in MTO reaction. Conversion (a,d) and colorimetric determination of HCHO concentration (b,c,e,f) versus time on stream for CH_3OH-N_2 and CH_3OH-H_2O cofeeding reactions over SAPO-34 at 723 K (a–c) and 548 K (d–f) with a methanol WHSV of 2.0 h^{-1}. The molecular molar ratio of methanol to water is 1:9 for reaction at 723 K, 1:1 and 1:3 for reactions at 548 K.

still detected in the CH_3OH-H_2O cofeeding reaction (Figs. 8(c) and 8(f)), and its amount was slightly lower than that in the CH_3OH-N_2 cofeeding reaction (Figs. 8(b) and 8(e)).

Our results provide direct experimental evidence for that HCHO can be partly eliminated by water cofeeding, partially contributing to the above effect of water cofeeding on MTO, and, however, this effect is not dominant, considering the considerable amount of HCHO in CH_3OH-H_2O cofeeding reaction. In fact, the effect of water on the MTO is very complex, and particularly, competitive adsorption between water, oxygenates, and HCPs has generally been used as a basis to rationalize the observed effects of water on MTO [59,72–74]. Specifically, it decreases the intrinsic reactivity of methanol and olefin and their accessibility to BASs, which attenuates many steps in the reaction network, including not only the generation of initial HCP, but also the dimerization, cyclization and HT of olefins (Fig. 3), thus prolonging the induction period and moderating the formation of coke [59,72–74].

3.5.2. *The effect of H_2 cofeeding on MTO reaction*

Next, we investigate the effect of H_2 cofeeding on MTO under high pressure. As shown in Fig. 9(a), a remarkably prolonged catalyst lifetime and reduced deactivation rate were observed in CH_3OH-H_2 cofeeding reaction comparing with CH_3OH-N_2 reaction over SAPO-34 at 723 K under 2 MPa, which are in line with the results reported by Bhan *et al.* [29,30] and our previous work [75]. Similar results also reported in syngas-to-olefins reaction *via* a dual-bed catalyst [78–80]. For high pressure MTO reaction, it is inevitable to use the stainless steel reactor, which is capable of decomposing methanol to HCHO [19]. In this work, plenty of HCHO was detected in the blank experiments conducted in an empty fixed-bed stainless steel reactor lined with a quart tube under identical reaction conditions (Fig. S15), which interferes with the evaluation of zeolite-catalyzed HCHO generation in the high-pressure MTO reactions. Nevertheless, a considerable quantity of HCHO was detected in CH_3OH-H_2 cofeeding reaction (Fig. 9(c)), which is similar to that in the CH_3OH-N_2 reaction (Fig. 9(b)), indicating that HCHO was not conspicuously reduced in MTO with high-pressure H_2 cofeeding.

Several plausible explanations have been proposed for the beneficial effects of H_2 on MTO lifetime: (1) hydrogenation of unsaturated HCPs such as alkenes, dienes (more favorable [30,76]) and aromatics [75,76], which attenuates aromatization process evoking by the cascade reactions of these species [30,75,76], i.e., product-induced HT reactions; (2) hydrogenation of HCHO, thereby suppressing HCHO-mediated deactivation process [29,30,76]; (3) decoking by high-pressure H_2 [75]. However, our results provide direct experimental evidence that high-pressure H_2 cofeeding does not conspicuously reduce HCHO in MTO reaction. The effect of H_2 on MTO is convoluted, except for the proposed hydrogenation of unsaturated species

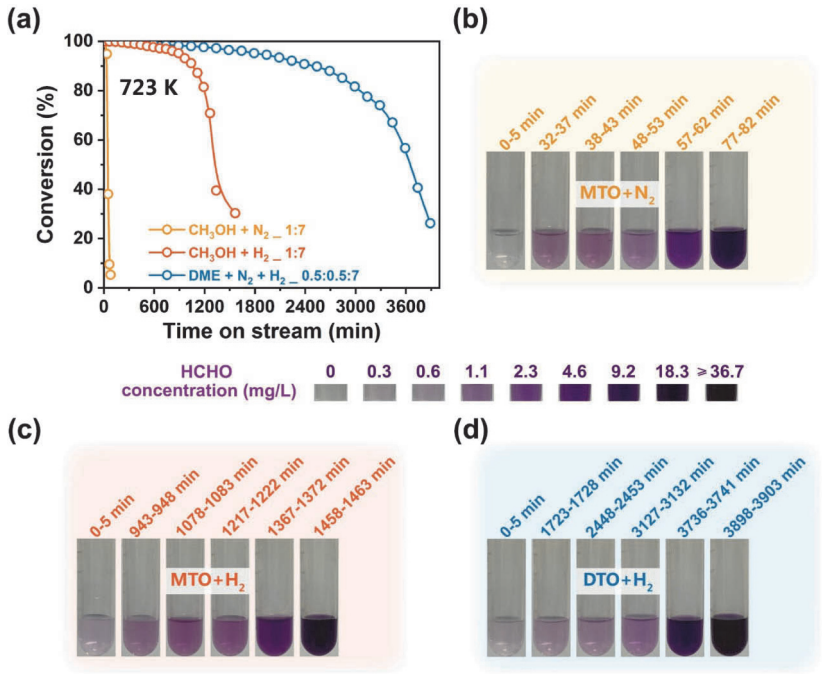

Fig. 9. Cofeeding high-pressure H_2 in MTO and DTO reaction. Conversion (a) and colorimetric determination of HCHO concentration (b–d) versus time on stream for CH_3OH-N_2 (molecular molar ratio 1:7), CH_3OH-H_2 (1:7) and DME-N_2-H_2 (0.5:0.5:7) cofeeding reactions over SAPO-34 at 723 K under 2 MPa. Reaction conditions: methanol WHSV is 4.0 h^{-1}, DME was fed with equimolar carbon amounts of methanol, GHSV is 11206.4 h^{-1}.

[29,30,75,76] and coke decoking [75], it is reasonable to speculate that high-pressure H_2 cofeeding may regulate the entire dynamic reaction network by suppressing HT reactions (Fig. 3), to achieve a moderate reaction course, thereby mitigating catalyst deactivation.

Based on the above understanding of high-pressure H_2 cofeeding effect, and further combined with our revelation of the two characteristics of DME-weak HT ability and moderate reaction kinetic [53], DME was used to replace methanol with high-pressure H_2 cofeeding to achieve a more moderate reaction course with depressed HT reaction and further improve the catalytic efficiency. Prospectively, compare to CH_3OH-H_2 cofeeding reaction, a more pronounced catalyst lifetime extension and deactivation rate reduction were achieved in high-pressure DME-H_2 cofeeding reaction (Fig. 9(a)).

4. Conclusions

This work uncovers the reactivity of methanol and DME for hydrogen transfer reactions over SAPO-34 and their effects on reaction network and catalyst deactivation. The effect of cofeeding water and high-pressure H_2 on MTO reaction are investigated based on the direct experimental evidence from the quantitative detection of HCHO.

By colorimetric analysis, the evolution of HCHO concentration throughout MTO and DTO processes was *in situ* quantitatively determined. Specifically, reactant-induced HT reactions are prominent during the initial and deactivation stages with semi-conversion, where slight and conspicuous amounts of HCHO were detected, mainly generated by the zeolite-catalyzed HT from methanol/DME to SMS and alkenes. Comparatively, product-induced HT reactions are dominant at highly efficient stage. Such dynamically evolving HT reactions as the hidden-line simultaneously occur and interplay with the main reactions of olefin generation as the open-line, constituting a complete dynamic reaction network of MTO and DTO. HT reactions are not only responsible for the generation of unsaturated active intermediates as autocatalyst, but also cause the coke deposition, which thus contributes to the dynamic evolution of autocatalytic network from initiating to decaying.

Even possessing the close reaction course, compared to MTO, the higher overall barrier of HT reactions for DME with weak HT ability in DTO reaction depresses the reactant-induced HT reactions and thus the generation of HCHO and alkanes, which enables relatively prominent olefins-based cycle, and manifests relatively moderate reaction and slow deactivation process. In contrast, methanol behaves both as H-acceptor (production of methane and H-poor species directly promoting coking process) and donor (production of HCHO inducing HCHO-mediated deactivation process) with strong HT ability, which exacerbates the competition between methylation and HT of methanol, and enables the reactant-induced deactivation pathway critical for MTO.

HCHO was still detected in the MTO and DTO reaction with water or high-pressure H_2 cofeeding. Importantly, cofeeding high-pressure H_2 with DME (instead of methanol) capacitates the modulation of dynamic reaction network to a more moderate autocatalysis evolution with depressed HT reaction, which was endowed by the weak HT ability and frustrated mass transfer (arousing low local chemical potential of reactant) [53] of DME and high-pressure H_2 effect. In this way, a long-term and highly efficient operation of DTO reaction with great potential in practical industrial application is achieved. These practice and knowledge are meaningful for the development

and application of efficient process and catalyst to fulfil the delicate control of the dynamic and complicated reaction network.

Author Contributions

S.L. conceived, coordinated the research, designed and conducted the experiments, and wrote the paper. Z.L. and Y.W. supervised the project, led the collaboration efforts, and revised the paper. Y.Z. participated in discussions and revised the paper. W.Z. contributed to the DFT calculations. X.Y. and M.Y. contributed to the deactivation model calculation. C.Z. helped in carrying out high-pressure reactions. S.X. performed the NMR characterization analysis. All authors contributed to interpreting the data and writing the manuscript.

Electronic supporting information

supporting information is available in the online version of this article, including: detailed calculations of the thermodynamic equilibrium molar fraction of CH_3OH and DME, other supplementary results and discussions of reaction and spectroscopy.

Declaration of Competing Interest

The authors declare no competing interests.

References

[1] P. Tian, Y. Wei, M. Ye, Z. Liu, *ACS Catal.*, **2015**, 5, 1922–1938.
[2] S. Xu, Y. Zhi, J. Han, W. Zhang, X. Wu, T. Sun, Y. Wei, Z. Liu, *Adv. Catal.*, **2017**, 61, 37–122.
[3] I. Yarulina, A. D. Chowdhury, F. Meirer, B. M. Weckhuysen, J. Gascon, *Nat. Catal.*, **2018**, 1, 398–411.
[4] S. Lin, Y. Zhi, W. Chen, H. Li, W. Zhang, C. Lou, X. Wu, S. Zeng, S. Xu, J. Xiao, A. Zheng, Y. Wei, Z. Liu, *J. Am. Chem. Soc.*, **2021**, 143, 12038–12052.
[5] S. Müller, Y. Liu, F. M. Kirchberger, M. Tonigold, M. Sanchez-Sanchez, J. A. Lercher, *J. Am. Chem. Soc.*, **2016**, 138, 15994–16003.
[6] S. Ilias, A. Bhan, *ACS Catal.*, **2013**, 3, 18–31.
[7] X. Sun, S. Mueller, Y. Liu, H. Shi, G. L. Haller, M. Sanchez-Sanchez, A. C. van Veen, J. A. Lercher, *J. Catal.*, **2014**, 317, 185–197.
[8] Y. Liu, F. M. Kirchberger, S. Müller, M. Eder, M. Tonigold, M. Sanchez-Sanchez, J. A. Lercher, *Nat. Commun.*, **2019**, 10, 1462.
[9] S. Müller, Y. Liu, M. Vishnuvarthan, X. Sun, A. C. van Veen, G. L. Haller, M. Sanchez-Sanchez, J. A. Lercher, *J. Catal.*, **2015**, 325, 48–59.
[10] G. J. Hutchings, F. Gottschalk, R. Hunter, *Ind. Eng. Chem. Res.*, **1987**, 26, 635–637.
[11] G. J. Hutchings, F. Gottschalk, M. V. M. Hall, R. Hunter, *J. Chem. Soc., Faraday Trans. 1*, **1987**, 83, 571–583.
[12] L. Kubelková, J. Nováková, P. Jírů, *Stud. Surf. Sci. Catal.*, **1984**, 18, 217–224.
[13] J. Nováková, L. Kubelková, Z. Dolejšek, *J. Catal.*, **1987**, 108, 208–213.
[14] P. N. Plessow, F. Studt, *ACS Catal.*, **2017**, 7, 7987–7994.
[15] Y. Liu, S. Müller, D. Berger, J. Jelic, K. Reuter, M. Tonigold, M. Sanchez-Sanchez, J. A. Lercher, *Angew. Chem. Int. Ed.*, **2016**, 55, 5723–5726.
[16] Z. Wei, Y.-Y. Chen, J. Li, P. Wang, B. Jing, Y. He, M. Dong, H. Jiao, Z. Qin, J. Wang, W. Fan, *Catal. Sci. Technol.*, **2016**, 6, 5526–5533.
[17] F. M. Kirchberger, Y. Liu, P. N. Plessow, M. Tonigold, F. Studt, M. Sanchez-Sanchez, J. A. Lercher, *Proc. Natl. Acad. Sci. U. S. A.*, **2022**, 119, e2103840119.
[18] J. S. Martinez-Espin, K. De Wispelaere, M. Westgård Erichsen, S. Svelle, T. V. W. Janssens, V. Van Speybroeck, P. Beato, U. Olsbye, *J. Catal.*, **2017**, 349, 136–148.
[19] J. S. Martinez-Espin, M. Mortén, T. V. W. Janssens, S. Svelle, P. Beato, U. Olsbye, *Catal. Sci. Technol.*, **2017**, 7, 2700–2716.
[20] J. S. Martínez-Espín, K. De Wispelaere, T. V. W. Janssens, S. Svelle, K. P. Lillerud, P. Beato, V. Van Speybroeck, U. Olsbye, *ACS Catal.*, **2017**, 7, 5773–5780.
[21] N. Tajima, T. Tsuneda, F. Toyama, K. Hirao, *J. Am. Chem. Soc.*, **1998**,

Graphical Abstract

Chin. J. Catal., 2023, 46: 11–27 doi: 10.1016/S1872-2067(22)64194-9

Hydrogen transfer reaction contributes to the dynamic evolution of zeolite-catalyzed methanol and dimethyl ether conversions: Insight into formaldehyde

Shanfan Lin, Yuchun Zhi, Wenna Zhang, Xiaoshuai Yuan, Chengwei Zhang, Mao Ye, Shutao Xu, Yingxu Wei *, Zhongmin Liu *
Dalian Institute of Chemical Physics, Chinese Academy of Sciences; University of Chinese Academy of Sciences

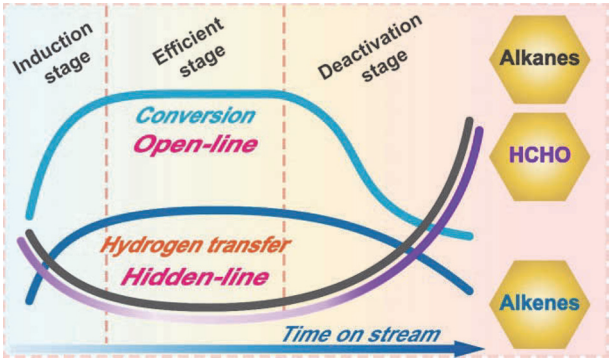

Dynamically evolving hydrogen transfer (HT) reactions as the hidden-line simultaneously occur and interplay with the main reactions of olefin generation as the open-line, constituting a complete dynamic reaction network for methanol and DME conversion. Modulating reaction network with depressing HT reactions for a moderate autocatalysis evolution is critical to realize a long-term and highly efficient reaction process.

120, 8222–8229.
[22] A. Comas-Vives, M. Valla, C. Copéret, P. Sautet, *ACS Cent. Sci.*, **2015**, 1, 313–319.
[23] Y. Chu, X. Yi, C. Li, X. Sun, A. Zheng, *Chem. Sci.*, **2018**, 9, 6470–6479.
[24] C. Wang, Y. Chu, J. Xu, Q. Wang, G. Qi, P. Gao, X. Zhou, F. Deng, *Angew. Chem. Int. Ed.*, **2018**, 57, 10197–10201.
[25] L. Yang, T. Yan, C. Wang, W. Dai, G. Wu, M. Hunger, W. Fan, Z. Xie, N. Guan, L. Li, *ACS Catal.*, **2019**, 9, 6491–6501.
[26] A. Hwang, A. Bhan, *Acc. Chem. Res.*, **2019**, 52, 2647–2656.
[27] B. L. Foley, B. A. Johnson, A. Bhan, *ACS Catal.*, **2021**, 11, 3628–3637.
[28] P. Bollini, T. T. Chen, M. Neurock, A. Bhan, *Catal. Sci. Technol.*, **2019**, 9, 4374–4383.
[29] S. S. Arora, D. L. S. Nieskens, A. Malek, A. Bhan, *Nat. Catal.*, **2018**, 1, 666–672.
[30] S. S. Arora, Z. Shi, A. Bhan, *ACS Catal.*, **2019**, 9, 6407–6414.
[31] A. Hwang, A. Bhan, *ACS Catal.*, **2017**, 7, 4417–4422.
[32] J. G. Dojahn, W. E. Wentworth, S. D. Stearns, *J. Chromatogr. Sci.*, **2001**, 39, 54–58.
[33] J. Nováková, L. Kubelkova, K. Habersberger, Z. Dolejšek, *J. Chem. Soc., Faraday Trans. 1*, **1984**, 80, 1457–1465.
[34] O. Dewaele, V. L. Geers, G. F. Froment, G. B. Marin, *Chem. Eng. Sci.*, **1999**, 54, 4385–4395.
[35] X. Wu, S. Xu, W. Zhang, J. Huang, J. Li, B. Yu, Y. Wei, Z. Liu, *Angew. Chem. Int. Ed.*, **2017**, 56, 9039–9043.
[36] W. Wen, S. Yu, C. Zhou, H. Ma, Z. Zhou, C. Cao, J. Yang, M. Xu, F. Qi, G. Zhang, Y. Pan, *Angew. Chem. Int. Ed.*, **2020**, 59, 4873–4878.
[37] J. Chen, J. Li, Y. Wei, C. Yuan, B. Li, S. Xu, Y. Zhou, J. Wang, M. Zhang, Z. Liu, *Catal. Commun.*, **2014**, 46, 36–40.
[38] M. J. Frisch, G. W. Trucks, H. B. Schlegel, G. E. Scuseria, M. A. Robb, J. R. Cheeseman, G. Scalmani, V. Barone, B. Mennucci, G. A. Petersson, H. Nakatsuji, M. Caricato, X. Li, H. P. Hratchian, A. F. Izmaylov, J. Bloino, G. Zheng, J. L. Sonnenberg, M. Hada, M. Ehara, K. Toyota, R. Fukuda, J. Hasegawa, M. Ishida, T. Nakajima, Y. Honda, O. Kitao, H. Naka, T. Vreven, J. A. Montgomery, J. E. Peralta, F. Ogliaro, M. Bearpark, J. J. Heyd, E. Brothers, K. N. Kudin, V. N. Staroverov, R. Kobayashi, J. Normand, K. Raghavachari, A. Rendell, C. J. Burant, S. S. Iyengar, J. Tomasi, M. Cossi, N. Rega, J. M. Millam, M. Klene, J. E. Knox, J. B. Cross, V. Bakken, C. Adamo, J. Jaramillo, R. Gomperts, R. E. Stratmann, O. Yazyev, A. J. Austin, R. Cammi, C. Pomelli, J. W. Ochterski, R. L. Martin, K. Morokuma, V. G. Zakrzewski, G. A. Voth, P. Salvador, J. J. Dannenberg, S. Dapprich, A. D. Daniels, O. Farkas, J. B. Foresman, J. V.Ortiz, J. Cioslowski, D. J. Fox, Gaussian 09, Revision B.01, Gaussian, Inc.: Wallingford, CT, **2010**.
[39] P. J. O'Malley, J. Dwyer, *Zeolites*, **1988**, 8, 317–321.
[40] J.-D. Chai, M. Head-Gordon, *Phys. Chem. Chem. Phys.*, **2008**, 10, 6615–6620.
[41] U. Olsbye, S. Svelle, M. Bjørgen, P. Beato, T. V. W. Janssens, F. Joensen, S. Bordiga, K. P. Lillerud, *Angew. Chem. Int. Ed.*, **2012**, 51, 5810–5831.
[42] GB/T 16129–1995.
[43] S. M. Campbell, X.-Z. Jiang, R. F. Howe, *Microporous Mesoporous Mater.*, **1999**, 29, 91–108.
[44] T. R. Forester, R. F. Howe, *J. Am. Chem. Soc.*, **1987**, 109, 5076–5082.
[45] S. A. Zubkov, L. M. Kustov, V. B. Kazansky, I. Girnus, R. Fricke, *J. Chem. Soc., Faraday Trans.*, **1991**, 87, 897–900.
[46] X. Wu, S. Xu, Y. Wei, W. Zhang, J. Huang, S. Xu, Y. He, S. Lin, T. Sun, Z. Liu, *ACS Catal.*, **2018**, 8, 7356–7361.
[47] I. B. Minova, S. K. Matam, A. Greenaway, C. R. A. Catlow, M. D. Frogley, G. Cinque, P. A. Wright, R. F. Howe, *ACS Catal.*, **2019**, 9, 6564–6570.
[48] J. D. Mosley, J. W. Young, J. Agarwal, H. F. Schaefer Iii, P. V. R. Schleyer, M. A. Duncan, *Angew. Chem. Int. Ed.*, **2014**, 53, 5888–5891.
[49] S. Shao, H. Zhang, R. Xiao, X. Li, Y. Cai, *J. Anal. Appl. Pyrolysis*, **2017**, 127, 258–268.
[50] S. R. Blaszkowski, R. A. van Santen, *J. Am. Chem. Soc.*, **1997**, 119, 5020–5027.
[51] J. Li, Z. Wei, Y. Chen, B. Jing, Y. He, M. Dong, H. Jiao, X. Li, Z. Qin, J. Wang, W. Fan, *J. Catal.*, **2014**, 317, 277–283.
[52] D. Lesthaeghe, V. Van Speybroeck, G. B. Marin, M. Waroquier, *Angew. Chem. Int. Ed.*, **2006**, 45, 1714–1719.
[53] S. Lin, Y. Zhi, Z. Liu, J. Yuan, W. Liu, W. Zhang, Z. Xu, A. Zheng, Y. Wei, Z. Liu, *Natl. Sci. Rev.*, **2022**, 9, nwac151.
[54] C. Peng, H. Wang, P. Hu, *Phys. Chem. Chem. Phys.*, **2016**, 18, 14495–14502.
[55] W. Zhang, Y. Zhi, J. Huang, X. Wu, S. Zeng, S. Xu, A. Zheng, Y. Wei, Z. Liu, *ACS Catal.*, **2019**, 9, 7373–7379.
[56] B. P. C. Hereijgers, F. Bleken, M. H. Nilsen, S. Svelle, K.-P. Lillerud, M. Bjørgen, B. M. Weckhuysen, U. Olsbye, *J. Catal.*, **2009**, 264, 77–87.
[57] S. Svelle, F. Joensen, J. Nerlov, U. Olsbye, K.-P. Lillerud, S. Kolboe, M. Bjørgen, *J. Am. Chem. Soc.*, **2006**, 128, 14770–14771.
[58] M. Bjørgen, S. Svelle, F. Joensen, J. Nerlov, S. Kolboe, F. Bonino, L. Palumbo, S. Bordiga, U. Olsbye, *J. Catal.*, **2007**, 249, 195–207.
[59] K. De Wispelaere, C. S. Wondergem, B. Ensing, K. Hemelsoet, E. J. Meijer, B. M. Weckhuysen, V. Van Speybroeck, J. Ruiz-Martínez, *ACS Catal.*, **2016**, 6, 1991–2002.
[60] K. Stanciakova, B. M. Weckhuysen, *Trends Chem.*, **2021**, 3, 456–468.
[61] P. N. Plessow, F. Studt, *Catal. Sci. Technol.*, **2018**, 8, 4420–4429.
[62] S. Svelle, B. Arstad, S. Kolboe, O. Swang, *J. Phys. Chem. B*, **2003**, 107, 9281–9289.
[63] S. Svelle, C. Tuma, X. Rozanska, T. Kerber, J. Sauer, *J. Am. Chem. Soc.*, **2009**, 131, 816–825.
[64] V. Van Speybroeck, J. Van der Mynsbrugge, M. Vandichel, K. Hemelsoet, D. Lesthaeghe, A. Ghysels, G. B. Marin, M. Waroquier, *J. Am. Chem. Soc.*, **2011**, 133, 888–899.
[65] S. Svelle, M. Visur, U. Olsbye, Saepurahman, M. Bjørgen, *Top. Catal.*, **2011**, 54, 897–906.
[66] J. Van der Mynsbrugge, S. L. C. Moors, K. De Wispelaere, V. Van Speybroeck, *ChemCatChem*, **2014**, 6, 1906–1918.
[67] R. Y. Brogaard, R. Henry, Y. Schuurman, A. J. Medford, P. G. Moses, P. Beato, S. Svelle, J. K. Nørskov, U. Olsbye, *J. Catal.*, **2014**, 314, 159–169.
[68] B. Arstad, S. Kolboe, O. Swang, *J. Phys. Chem. B*, **2002**, 106, 12722–12726.
[69] U. Olsbye, S. Svelle, K. P. Lillerud, Z. H. Wei, Y. Y. Chen, J. F. Li, J. G. Wang, W. B. Fan, *Chem. Soc. Rev.*, **2015**, 44, 7155–7176.
[70] J. F. Haw, D. M. Marcus, *Top. Catal.*, **2005**, 34, 41–48.
[71] S. V. Konnov, V. S. Pavlov, P. A. Kots, V. B. Zaytsev, I. I. Ivanova, *Catal. Sci. Technol.*, **2018**, 8, 1564–1577.
[72] A. J. Marchi, G. F. Froment, *Appl. Catal. A*, **1993**, 94, 91–106.
[73] A. J. Marchi, G. F. Froment, *Appl. Catal.*, **1991**, 71, 139–152.
[74] H. Wang, Y. Hou, W. Sun, Q. Hu, H. Xiong, T. Wang, B. Yan, W. Qian, *ACS Catal.*, **2020**, 10, 5288–5298.
[75] X. Zhao, J. Li, P. Tian, L. Wang, X. Li, S. Lin, X. Guo, Z. Liu, *ACS Catal.*, **2019**, 9, 3017–3025.
[76] M. DeLuca, C. Janes, D. Hibbitts, *ACS Catal.*, **2020**, 10, 4593–4607.
[77] X. Wu, R. G. Anthony, *Appl. Catal. A*, **2001**, 218, 241–250.
[78] Z. Liu, Y. Ni, X. Fang, W. Zhu, Z. Liu, *J. Energy Chem.*, **2021**, 58, 573–576.

[79] Y. Ni, Z. Liu, P. Tian, Z. Chen, Y. Fu, W. Zhu, Z. Liu, *J. Energy Chem.*, **2022**, 66, 190.

[80] Y. Ni, Y. Liu, Z. Chen, M. Yang, H. Liu, Y. He, Y. Fu, W. Zhu, Z. Liu, *ACS Catal.*, **2019**, 9, 1026–1032.

氢转移反应对分子筛催化甲醇和二甲醚动态自催化反应历程的贡献：深入理解甲醛的生成机理和作用机制

林杉帆[a,c], 郅玉春[a], 张文娜[a], 袁小帅[d], 张成伟[a,c], 叶 茂[a], 徐舒涛[a], 魏迎旭[a,*], 刘中民[a,b,c,*]

[a]中国科学院大连化学物理研究所, 低碳催化技术国家工程研究中心, 洁净能源国家实验室, 能源材料化学协同创新中心, 辽宁大连116023

[b]中国科学院大连化学物理研究所, 催化基础国家重点实验室, 辽宁大连116023

[c]中国科学院大学, 北京100049

[d]中国科学院大连化学物理研究所, 能源战略研究中心, 辽宁大连116023

摘要: 甲醇制烯烃(MTO)已成为从非石油资源获取低碳烯烃的最为成功的工业化路线, 受到学术界和工业界的广泛关注. MTO反应是一个动态的自催化过程, 其中烯烃、甲基环戊烯和芳烃物种作为(自)催化剂. 氢转移(HT)反应是构建MTO自催化剂和烷烃副产物的主要途径, 对于深入理解MTO反应的动态特性及其复杂反应网络至关重要. 作为反应物甲醇/二甲醚发生HT反应的产物, 甲醛对MTO反应中自催化的引发和失活具有重要作用. 然而, 由于甲醛的反应活性高、浓度低且对色谱FID检测器的灵敏度低, 因此甲醛难以像其它烃类产物一样通过常规手段进行在线定量监测, 迄今甲醛在整个反应过程中的演变规律仍不清楚, 这阻碍了对反应物诱导的HT反应以及整个反应网络的全面认识.

本文借助实验及理论计算研究了SAPO-34分子筛上甲醇和二甲醚转化过程中的HT反应, 尤其是生成甲醛的反应物诱导的HT反应. 首先, 建立了一种定量检测甲醛的实验方法, 实现在真实反应条件下, 原位定量监测整个MTO和二甲醚制烯烃(DTO)过程中甲醛浓度的变化. 在此基础上, 将甲醛浓度变化规律与其它反应规律关联起来, 更为详细地追踪整个反应过程中H原子的轨迹, 并进一步结合DFT计算、operando光谱分析、$^{12}C/^{13}C$同位素切换、失活动力学分析, 研究了MTO/DTO不同反应阶段中甲醛的生成机理, 揭示了甲醇和二甲醚的甲基化活性和氢转移活性, 及其对反应网络和积碳失活的影响, 从而确定了MTO和DTO反应的失活机理和模型. 结合甲醛的定量检测, 还研究了共进料H_2O和高压H_2对MTO/DTO反应的影响. 综合上述信息, 提出减缓催化剂积碳失活的策略, 并加以实践应用.

反应物诱导的HT反应在反应物未能完全转化的初始阶段和失活阶段尤为突出, 两个阶段检测到少量和大量的甲醛, 分别主要由分子筛催化的甲醇/二甲醚与甲氧基和烯烃之间的HT反应产生; 而产物诱导的HT反应在高效反应阶段占主导地位. 这种动态演变的HT反应作为“暗线”与作为“明线”的烯烃生成的主反应同时发生并相互作用, 共同构成MTO和DTO完整的动态反应网络. HT反应不仅能够生成作为自催化剂的不饱和活性中间体, 而且能够生成积碳并导致失活, 对MTO自催化网络从启动到衰退的动态演变起到关键作用.

DTO反应中, 由于二甲醚的HT反应能力较弱, 参与HT反应的能垒较高, 因此, 反应物诱导的HT反应受到抑制, 相应的甲醛、烷烃以及缺氢物种的生成相对受到抑制, 这使得DTO反应中烯烃循环相对突出, 并表现出相对温和的反应历程和缓慢的失活过程. 相比之下, 甲醇具有很强的HT能力: 一方面作为氢受体生成甲烷和缺氢物种, 直接参与并促进积碳失活的发生；另一发面, 作为氢供体生成甲醛, 引发甲醛介导的失活过程, 间接参与并促进积碳生成. 同时, 甲醇较强的HT能力加剧了甲醇甲基化反应与HT反应之间的竞争, 使得反应物诱导的HT和失活过程在MTO反应中至关重要. 共进料H_2O和高压H_2的MTO/DTO反应中仍然能够检测到甲醛, 且含量略小于或者等于非共进料体系.

特别指出，HT能力较弱和传质受限引起局部催化微环境中反应物的化学势较低是二甲醚反应的两大特点. 共进料高压H_2对MTO反应的影响包括不饱和烃类物种的加氢、加氢消碳和抑制HT反应的发生. 利用上述两点对反应机理的理解, 采用二甲醚(而不是甲醇)与高压H_2共进料, 可进一步使得反应过程中的HT反应受到抑制, 进而调节动态反应网络以更温和的自催化演变方式发生, 实现反应高效且长周期的运行, 该反应过程具有实际工业应用潜力.

综上, 本工作的研究和实践尝试对于高效的工艺和催化剂的开发和应用, 并以此实现对动态复杂反应网络的精准调控具有重要意义.

关键词: 甲醇制烯烃; 二甲醚; 氢转移; 甲醛; 失活

收稿日期: 2022-09-26. 接受日期: 2022-11-10. 上网时间: 2023-03-05.

*通讯联系人. 电子信箱: liuzm@dicp.ac.cn (刘中民), weiyx@dicp.ac.cn (魏迎旭).

基金来源: 国家自然科学基金(21991092, 21991090, 22072148, 21703239, 22002157); 大连化物所创新研究基金(DICP I202121); 辽宁省自然科学基金(2022-MS-029); 中国科学院前沿科学重点研究计划(QYZDY-SSW-SC024).